Clay Minerals (1984) **19**, 541–561

DIFFRACTION EFFECTS CALCULATED FOR STRUCTURAL MODELS OF K-SATURATED MONTMORILLONITE CONTAINING DIFFERENT TYPES OF DEFECTS

V. A. DRITS, A. PLANÇON*, B. A. SAKHAROV, G. BESSON*, S. I. TSIPURSKY AND C. TCHOUBAR*

*Geological Institute of USSR Academy of Sciences, Pyzhewsky 7, Moscow 1999017, USSR, and *Laboratory of Crystallography* (ERA no. 841), *University of Orleans, 45046 Orleans Cedex, France*

(*Received 5 December 1983*)

ABSTRACT: The general approach to the problem of the real structure of smectites requires an analysis based on the relationship between structural characteristics and diffraction patterns. This paper, which considers only the models corresponding to dioctahedral smectites saturated by K-cations and collapsed, includes: 1. Successive consideration of all models which are crystallochemically possible. These models may differ in (i) the structure and chemical composition of layers and interlayer spaces; (ii) the azimuthal orientations, translations and the mode of alternation of the layers; (iii) independent parameters which describe quantitatively the models (e.g. abundance of each type of layer, probability parameters defining the succession of layers, . . .). 2. Calculation, in all accessible domains of reciprocal space, of the distribution of intensities and profile variations, obtained by changing only one parameter at a time, that defines one type of structural feature (e.g. cation distribution in individual layers, stacking of the layers, nature of stacking faults, . . .). 3. A systematical analysis of the calculated diffraction patterns to establish the diffraction criteria which will help to interpret the experimental data explicitly.

In dioctahedral smectites only two of the three possible octahedral sites in the half unit cell are occupied by cations. These smectites are classified into montmorillonites, beidellites and nontronites, according to the composition of tetrahedral and octahedral sheets and the magnitude of the negative charge on the layer. To describe the crystal structure of smectites requires knowledge of (i) the composition and structure of the layers and interlayer spaces and (ii) the orientation and succession of these structural elements. For natural samples determination of both (i) and (ii) is usually difficult due to the small size of the particles and poor structural ordering. Normally, diffraction patterns of smectites contain only two types of reflections: basal 00*l* reflections and practically unmodulated (*hk*) bands corresponding to a two-dimensional diffraction. Obviously such data are not enough for a detailed determination of crystallochemical and structural characteristics of smectites. Determination of the internal structure of the 2:1 layers can be aided by a better ordering of layer stacking. For example, Mamy & Gaultier (1976) pointed out that montmorillonite shows a better ordering of layer stacking after K-saturation and several wetting and drying cycles (WD cycles), the resulting X-ray patterns contain strong reflections which have been indexed in a monoclinic one-layer unit cell. Based on selected-area electron diffraction results these authors supposed that after WD treatment

the layers have the same orientation instead of being rotated at random as in natural minerals. Similarly, Tsipursky *et al.* (1976) established that K-saturation of nontronites improved their structural ordering.

During the same period a number of quantitative studies were carried out which were based on comparisons of experimental intensity profiles with calculated ones for different models. This method was applied by Plançon *et al.* (1978) to establish the nature and proportions of stacking faults in K-montmorillonite after different WD cycles, while Besson (1980) and Besson *et al.* (1983) used it for several montmorillonites and beidellites saturated by Li^+, Na^+, K^+, Rb^+ and Cs^+. Particularly, Besson's work established that: (i) stacking ordering improves with increase in tetrahedral charge and the radius of the interlamellar cation; (ii) Cs-exchange without WD cycles has the same effect on the ordering of layer stacking as K-saturation after WD cycles; (iii) in the montmorillonites and also some of the beidellites studied the octahedral *cis* positions were vacant, while the Black Jack Mine beidellite was characterized by *trans*-vacant positions (Güven & Pease, 1975).

Recently, a more systematic but semi-quantitative study was made by Tsipursky (1982) in a structural investigation of dioctahedral smectites with different compositions and genesis. Using a WD treatment for K-saturated minerals, and indexing the positions and intensities of *hkl* reflections from oblique-texture electron diffraction patterns (for the first and second ellipses), this author concluded that the stacking of layers in K-smectites is the same as that in mica. He also showed that among dioctahedral smectites there are species in which: (i) *trans* positions are vacant (all the studied nontronites and some montmorillonites); (ii) one of the two kinds of *cis* positions is vacant (most of the montmorillonites and some beidellites); (iii) all octahedral positions are occupied with a 2/3 probability (some beidellites). In addition he found some intermediate cases for *cis* and *trans* octahedra occupation (some montmorillonites).

All these results agree in principle with several previous conclusions (Mering & Oberlin, 1967; Güven & Pease, 1975; Brindley & Brown, 1980) and give firm information on fine structural features of dioctahedral smectites. However, until recently, quantitative determination of structural characteristics of smectites has been based on only a few examples. It would be instructive to adopt a more general approach to the problem of the real structure of smectites based on a systematic analysis of the relationship between structural characteristics and diffraction patterns. Such a general approach, whose efficiency has been demonstrated by Drits & Sakharov (1976) for mixed-layer minerals, should include:

1. Successive consideration of all models which are crystallochemically possible. These models may differ in (i) the structure and chemical composition of layers and interlayer spaces; (ii) the azimuthal orientations, translations and mode of alternation of the layers; (iii) independent parameters which describe quantitatively the models (e.g. abundance of each type of layer, probability parameters defining the succession of layers, . . .).
2. Calculation, in all accessible domains of reciprocal space, of the distribution of intensities and profile variations obtained by changing only one parameter at a time, that defines one type of structural feature (e.g. cation distribution in individual layers, layer stacking, nature of stacking faults, . . .).
3. A systematical analysis of the calculated diffraction patterns to establish the diffraction criteria which will help to interpret the experimental data explicitly.

4. Refinement of experimental conditions to reveal special crystallochemical features among different theoretical possibilities.

This is the aim of this paper which considers only the models corresponding to dioctahedral smectites saturated by K-cations and collapsed (anhydrous state).

MODEL DESCRIPTIONS

Definition

Let us consider models equivalent to the $1M$ polytype of dioctahedral mica with a monoclinic unit cell, and stackings in which all layers have the same azimuthal orientation and hexagonal cavities are face to face. We will assume that such stacking models can be obtained with several types of layers that will differ in cation distribution over octahedral sites, namely, layers in which *trans* positions are vacant (named T layers), layers in which one of the two of *cis* positions are vacant (C_1 and C_2 layers), and layers in which all octahedral sites are randomly occupied either with the same $\frac{2}{3}$ probability (M layers) or with different probabilities.

Note that a random occupancy of the three types of octahedral sites can be described in two possible ways:

1. Distribution of cations among all octahedral positions in each layer is a true random distribution.
2. Each individual layer contains different domains in which octahedral cation distribution is strictly regular but which differ in the nature of vacant positions, forming domains of T, C_1 or C_2 types. The stacking of layers of this kind (named I stacking) may be considered, to a first approximation, as a mixed-layer structure with random alternation of T, C_1 and C_2 layers in equal or different abundances (with either a statistical $\frac{2}{3}$ probability or not). Further on, one of the problems will be to examine if it is possible to distinguish the diffraction patterns given by such a mixed-layer stacking from those given by a stacking with really random distribution of octahedral cations in each layer.

Structural features and regular stackings of the T, C_1 and C_2 layers

Fig. 1a represents a projection of a *trans*-vacant octahedral sheet with anions corresponding to the upper roof of the octahedra. Arrows show the direction of anion

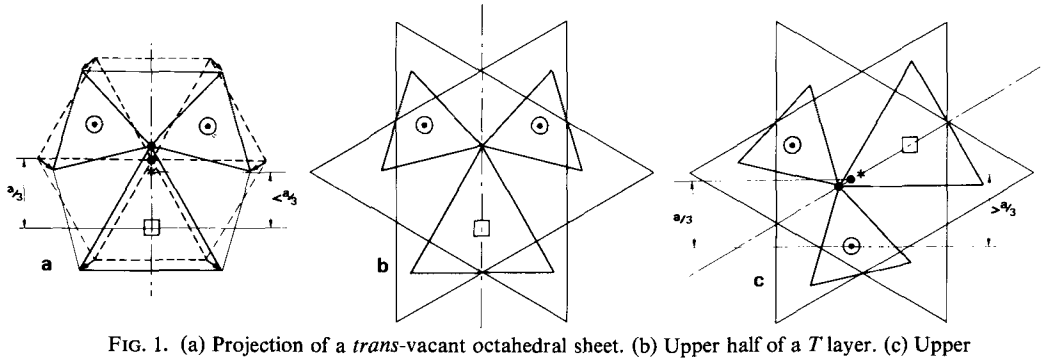

FIG. 1. (a) Projection of a *trans*-vacant octahedral sheet. (b) Upper half of a T layer. (c) Upper half of a C layer.

displacements caused by the screening of electrostatic cation repulsion (Bailey, 1966): regular hexagons are transformed into irregular hexagons with two long and four short sides. At the same time, the centre of the distorted hexagon (marked by an asterisk) shifts along the a axis towards the centre of a vacant octahedral *trans* position, and, consequently, the distances between these two points becomes smaller than $a/3$. Then, in mica-like stacking of T layers (named T-stacking), the modulus of the projection of the c axis on the $(\vec{a},\vec{b})$ plane is greater than $a/3$. This holds true when in interlayers the hexagonal cavity centres of the adjacent layers coincide in the projection on the $(\vec{a},\vec{b})$ plane.

The upper half of a T layer is shown in Fig. 1b, while Fig. 1c shows the upper half of a C layer. If cation compositions of these T and C layers are the same, we may assume that their octahedral distortions will also be the same. Moreover if we ignore the presence of OH groups in different positions, we can deduce that the upper half of a C_1 or C_2 layer is obtained by a $\pm 120°$ rotation of a half of a T layer around an axis passing through the OH group and perpendicular to the half-layer plane. It should be remembered that in the obtained half of a C layer the centre of the distorted hexagon is separated from the centre of the *trans* octahedron by a distance greater than $a/3$; consequently, in a mica-like stacking of C layers (named C-stacking), the modulus of the projection of the c axis on the $(\vec{a},\vec{b})$ plane is smaller than $a/3$.

Then, the knowledge of unit cell parameters and atomic coordinates for a T layer permits us to calculate easily the atomic coordinates of the upper half of a C_1 or C_2 layer. The lower half is obtained through rotation around a two-fold axis parallel to the b axis and passing through the centre of the *trans* octahedron. This method of determination of unit-cell parameters and atomic coordinates for a C layer is illustrated in Table 1 which

TABLE 1. Atomic coordinates for each type of layer.

	T layer			C_1 layer			M layer		
Atoms	x	y	z	x	y	z	x	y	z
O_1	0·615	0·691	0·608	0·730	−0·655	0·608	0·667	0·667	0·608
O_2	0·615	0·309	0·608	0·656	−0·347	0·608	0·667	0·333	0·608
O_3	0·667	0·500	0·820	0·732	−0·496	0·835	0·710	0·500	0·830
O_4	0·352	0·728	0·835	0·416	−0·725	0·820	0·395	0·728	0·830
O_5	0·352	0·272	0·835	0·416	−0·268	0·835	0·395	0·272	0·830
O_6	0·002	0·691	0·392	−0·038	−0·655	0·392	0·000	0·667	0·392
O_7	0·002	0·309	0·392	0·036	−0·347	0·392	0·000	0·333	0·392
O_8	−0·050	0·500	0·180	−0·040	−0·496	0·165	−0·044	0·500	0·170
O_9	0·264	0·728	0·165	0·275	−0·725	0·180	0·272	0·728	0·170
O_{10}	0·264	0·272	0·165	0·276	−0·268	0·165	0·272	0·272	0·170
OH_1	0·687	0·000	0·608	0·656	0·035	0·608	0·667	0·000	0·608
OH_2	−0·070	0·000	0·392	0·035	0·035	0·392	0·000	0·000	0·392
Si_1	0·622	0·329	0·770	0·683	−0·333	0·770	0·667	0·333	0·770
Si_2	0·622	0·671	0·770	0·695	−0·662	0·770	0·667	0·667	0·770
Si_3	−0·005	0·329	0·230	0·008	−0·333	0·230	0·000	0·333	0·230
Si_4	−0·005	0·671	0·230	−0·003	−0·662	0·230	0·000	0·667	0·230
Al_1	0·308	0·333	0·500				0·333	0·333	0·500
Al_2	0·308	0·667	0·500	0·346	−0·321	0·500	0·333	0·667	0·500
Al_3				0·346	0·0124	0·500	0·333	0·000	0·500
K_1	0·617	0·000	1·000	0·691	0·000	1·000	0·667	0·000	1·000
K_2	0·000	0·000	0·000	0·000	0·000	0·000	0·000	0·000	0·000

presents a specific case of the refined structure of a mica (Tsipursky & Drits, 1977). The structural formula of this mica is: $K_{0.8}[Si_{3.5}Al_{0.5}][Al_{1.70}Mg_{0.30}]O_{10}(OH)_2$, and cell parameters are $a = 5{\cdot}199$ Å, $b = 9{\cdot}005$ Å, $c = 10{\cdot}164$ Å and $\beta = 101{\cdot}3°$, giving $t_0 = c \cos \beta = -0{\cdot}383a$ ($> -a/3$). The atomic coordinates (T layer) of this mica are given in columns 1, 2 and 3, while the calculated atomic coordinates of the corresponding C_1 layer are reported in columns 4, 5 and 6; the new unit-cell parameters are: $a = 5{\cdot}199$ Å, $b = 9{\cdot}005$ Å, $c = 10{\cdot}09$ Å, $\beta = 99{\cdot}13°$, giving $t_0 = c \cos \beta = -0{\cdot}308\ a$ ($< -a/3$). Similarly, we have obtained the atomic coordinates of a M layer, which presents a real random distribution of cations with a $\frac{2}{3}$ probability of occupancy of each type of octahedral sites (see columns 7, 8 and 9, Table 1), through averaging the coordinates corresponding to T, C_1 and C_2 layers. The corresponding unit-cell parameters for M stacking are: $a = 5{\cdot}199$ Å, $b = 9{\cdot}005$ Å, $c = 10{\cdot}12$ Å, $\beta = 99{\cdot}86°$; in this case $t_0 = c \cos \beta = -a/3$.

Models containing different types of defects

Defects by rotations of layers in the stacking. Mica-like stacking may lead to azimuthal defects corresponding to $\pm 120°$ or $n60°$ rotations of successive layers. When stacking faults are $\pm 120°$ the usual octahedral coordination of K cations is preserved. In the case of 60°, 180° or 300° rotation of adjacent layers, K cations have prismatic coordination. So the existence of $n60°$ rotational defects leads to different coordinations of interlayer cations*.

It should be noted that the existence of rotation defects introduces new directions for interlayer displacements. These displacements correspond to rotating the t_0 translation by $n60°$ or $\pm 120°$. Moreover, because the (a, b) unit cell is centered, two of $\pm 120°$ rotated adjacent layers in a T stacking where $\vec{t}_0 > -\vec{a}/3$ are shifted along $\vec{a}$ by a value smaller than $-a/3$, while this displacement is greater than $-a/3$ for two rotated adjacent layers in a C stacking. In the case of 60°–180°–300° rotations these displacements for rotated adjacent layers are oriented in the positive $\vec{a}$ direction.

Defects by translational stacking faults. Three groups of translational defects have been considered: faults by $\pm\vec{b}/3$ or $-\vec{a}/3$ or $-\vec{a}/3 \pm \vec{b}/3$ translations.

Let us consider a model containing only $\pm\vec{b}/3$ stacking faults. For Cs-saturated beidellite Besson (1980, 1983) showed that such stacking faults led to an increase in the thickness of the interlayer space. To describe such a model it is necessary to use two different basal distances as in the case of a mixed-layer structure. In the case of a K-saturated smectite the values of the two basal distances introduced by the $\pm\vec{b}/3$ faults depend on the chemical composition of the mineral which modifies the value of the angle of rotation of tetrahedra.

The presence of the $\pm\vec{b}/3$ faults leads to a symmetrical surrounding of K cations by oxygen atoms. Such a configuration gives a high concentration of negative charges near K cations and, from a crystallochemical point of view, this situation may not be energetically favourable. For this reason we have also considered models with translational $-\vec{a}/3 \pm \vec{b}/3$ faults which lead to layer stackings like those in pyrophyllite.

* From a purely theoretical point of view, it is possible to obtain rotational $n60°$ defects with only octahedral coordinations of K cations if each $n60°$ rotated layer ($n = 1, 3, 5$) presents a rotation of tetrahedra in the direction opposite to that of T or C layers, described in Fig. 1. But the distribution of intensities calculated for this type of model differs considerably from all known experimental data on micas and smectites. Therefore, we do not consider such models in this paper.

The studied models of the last type contain $-n\vec{a}/3 \pm m\vec{b}/3$ stacking faults (with $n = 0$ or 1 and $m = 0$ or 1) which constitute a general case obtained by combination of the three groups of translational defects: $\pm\vec{b}/3, -\vec{a}/3$ and $-\vec{a}/3 \pm \vec{b}/3$.

We must emphasize that in the case of the models with $\pm\vec{b}/3$ and $-n\vec{a}/3 \pm m\vec{b}/3$ translational defects the sets of interlayer translations are the same as in the models with $\pm 120°$ and $n60°$ rotational defects respectively.

Mixed-layer models with T, C_1 and C_2 layers. To describe a statistical occupancy of all octahedral sites, models with randomly alternating T, C_1 and C_2 layers (I stackings) can be considered as more favourable from a crystallochemical point of view. In contrast to a pure random octahedral occupancy in each layer random *alternation* considered here permits a local electro-neutrality in each T or C domain.

Interstratification of T, C_1 and C_2 layers brings about two interlayer displacements. For the above described mica-like mineral these two displacements are:

$$\vec{t}_{TT} = \vec{t}_{TC_1} = \vec{t}_{TC_2} = -0{\cdot}383\vec{a} + \vec{n}d_{001}$$

and

$$\vec{t}_{C_1T} = \vec{t}_{C_1C_1} = \vec{t}_{C_1C_2} = \vec{t}_{C_2T} = \vec{t}_{C_2C_2} = \vec{t}_{C_2C_1} = -0{\cdot}308\vec{a} + \vec{n}d_{001}$$

where $\vec{n}$ is the unit vector normal to the $(\vec{a}, \vec{b})$ plane and $d_{001} = c \sin\beta = 9{\cdot}967$ Å.

Models with arbitrary translational faults and models with narrow distribution around average values. In all the models studied in this investigation we have introduced random defects due to some proportion of adjacent layers with arbitrary mutual translations (as is well described in the literature).

On the other hand we have also considered the case when translations between adjacent layers are not exactly equal to definite fractions of $\vec{a}$ or $\vec{b}$ but fall within a narrow range of these definite values.

MATHEMATICAL FORMALISM FOR CALCULATIONS

The mathematical formalisms used to characterize the studied models have been described in various papers (Plançon, 1976; Plançon & Tchoubar, 1976, 1977a, b; Besson, 1980; Plançon, 1981; Sakharov *et al.*, 1982 a, b). They permit one to obtain the continuous distribution of intensities either along individual *hk* rods or for powder diffraction patterns, which can be directly compared with experimental data.

DESCRIPTION OF THE INTENSITY DISTRIBUTION OBTAINED FOR DIFFERENT MODELS

The intensity distribution will be described for models with T, C, M and I stackings, and, to begin with, we will analyse the diffraction features of these models without any stacking faults. Then we will distinguish three main families of faults to take into account their specificity in the modification of the intensity distribution:

1. Stackings containing only arbitrary defects without any 'semi-defined' rotational or translational faults (we define as 'semi-defined' such faults as $\pm n60°$ or $-n\vec{a}/3 \pm m\vec{b}/3$).
2. Stackings containing semi-defined faults which strongly modify the distribution of intensity for *hk* reflections with $k \neq 3n$ (these are $\pm 120°$ or $\pm\vec{b}/3$ faults).

3. Stackings with semi-defined faults which modify all *hkl* reflections except 00*l* ones (these are $\pm n60°$ faults with n odd or $-n\vec{a}/3 \pm m\vec{b}/3$ faults with n and m integers).

Intensity distribution for T, C, M and I stackings without any stacking faults

Table 2 compares the intensities in the maxima of $02l, 11l$ and $20l, 13l$ reflections calculated for such stackings in the case of a single crystal, while in Figs 2, 3, 4 and 5 we give the corresponding reflection profiles in the case of powder diagrams. We have chosen for all stackings the same mean value $\bar{N}$ for the number of layers ($\bar{N} = 20$) and radius R for the coherent domain in the $(\vec{a}, \vec{b})$ plane equal to 200 Å.

The comparison between calculated profiles and also between intensities in Table 2 shows that in the absence of stacking faults each model gives a specific diffraction profile and can be distinguished from the others.

It can be observed that:

1. The series of $02l, 11l$ reflections shows that in T stacking the $\bar{1}\bar{1}1$, $\bar{1}\bar{1}2$ and 112 reflections are more intense than the 111, 022 and $\bar{1}\bar{1}3$ reflections while in C stacking the 022 and $\bar{1}\bar{1}3$ reflections become more intense than the others. In M stacking the most intense reflections are 022, 112 and $\bar{1}\bar{1}3$. Therefore the occupancy of *trans* octahedral sites is the main factor that influences the distribution of these reflection intensities. For I stacking the more intense reflections are those of M stacking but, compared with the latter,

TABLE 2. Intensities of the (*hkl*) reflections for each stacking model (without stacking faults).

h k l	*T* stacking	*C* stacking	*M* stacking	*I* stacking
0 2 2	35 051	122 120	86 756	81 842
0 2 1	12 608	18 377	—	—
0 2 0	157 350	44 251	52 550	59 730
1 1 2	164 220	79 086	100 520	80 096
1 1 1	—	39 705	13 237	12 828
1 1 0	1 655	99 054	40 244	37 783
$\bar{1}\,\bar{1}$ 3	46 354	113 870	83 690	71 427
$\bar{1}\,\bar{1}$ 2	110 950	33 064	49 475	39 196
$\bar{1}\,\bar{1}$ 1	69 809	17 486	14 944	12 078
2 0 2	104 970	101 010	118 900	51 128
2 0 1	166 700	120 330	147 980	65 288
2 0 0	130 680	148 720	144 130	70 105
$\bar{2}$ 0 3	37 479	30 118	25 117	15 567
$\bar{2}$ 0 2	69 431	76 102	89 415	36 906
$\bar{2}$ 0 1	62 459	57 587	68 078	27 806
1 3 2	30 117	33 973	25 121	26 778
1 3 1	76 104	73 316	89 459	60 625
1 3 0	57 587	60 234	68 070	18 729
$\bar{1}\,\bar{3}$ 3	101 010	105 930	118 180	81 498
$\bar{1}\,\bar{3}$ 2	120 330	141 770	147 900	108 730
$\bar{1}\,\bar{3}$ 1	148 720	138 620	144 050	115 750

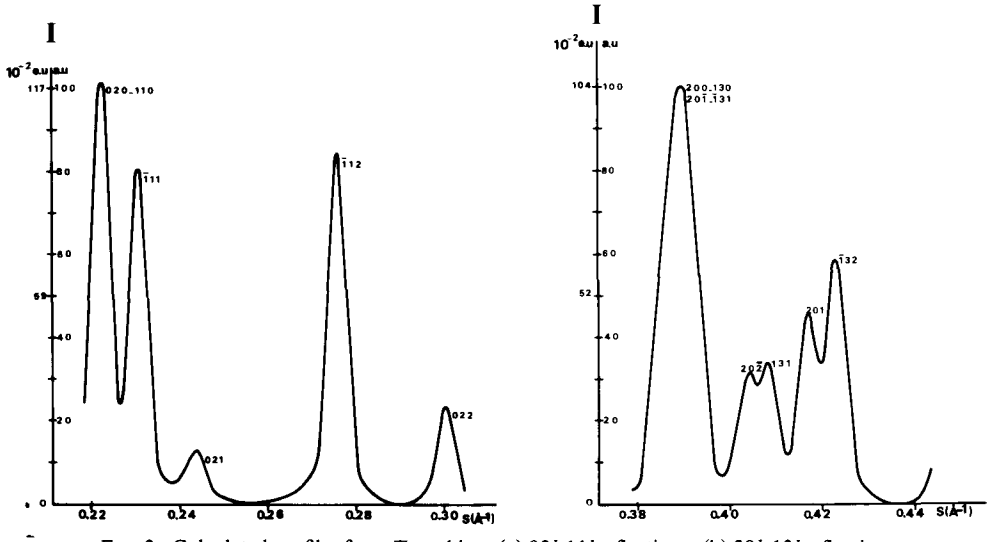

FIG. 2. Calculated profiles for a T stacking: (a) $02l$, $11l$ reflections; (b) $20l$, $13l$ reflections.

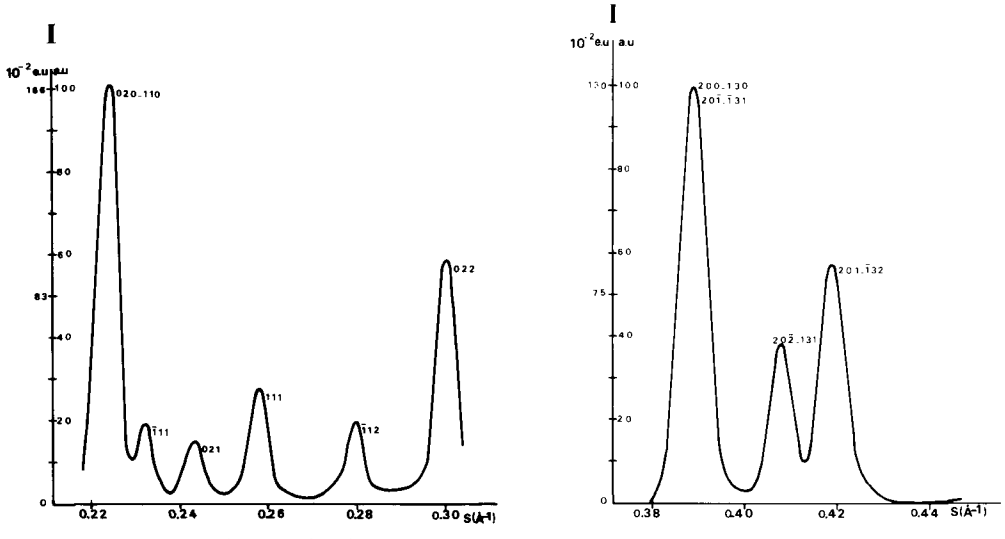

FIG. 3. Calculated profiles for a C stacking: (a) $02l$, $11l$ reflections; (b) $20l$, $13l$ reflections.

they differ much in their relative and absolute intensities in powder patterns. The differences in relative intensities are related to the use of one single interlayer $\vec{t}_0 = -\vec{a}/3$ translation for M stacking and two different translations ($\vec{t}'_0 = -0{\cdot}383\vec{a}$ and $\vec{t}''_0 = -0{\cdot}308\vec{a}$) for I stacking.

2. In the series of $20l$, $13l$ reflections a large difference appears in powder diagrams between T stacking, on the one hand, and C, M and I stacking on the other. In the first case we observe five modulations while in the other cases there are only three. This

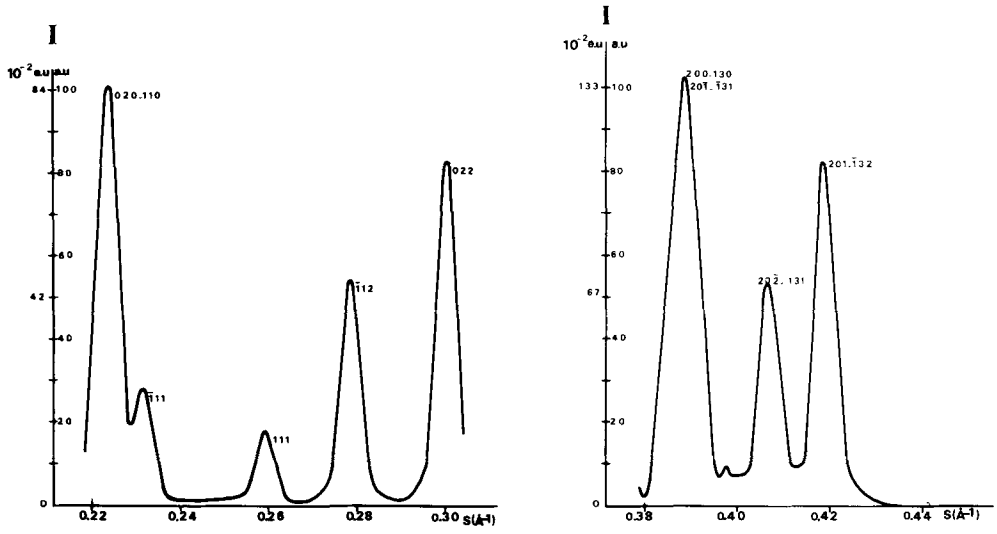

FIG. 4. Calculated profiles for an *M* stacking: (a) 02*l*, 11*l* reflections; (b) 20*l*, 13*l* reflections.

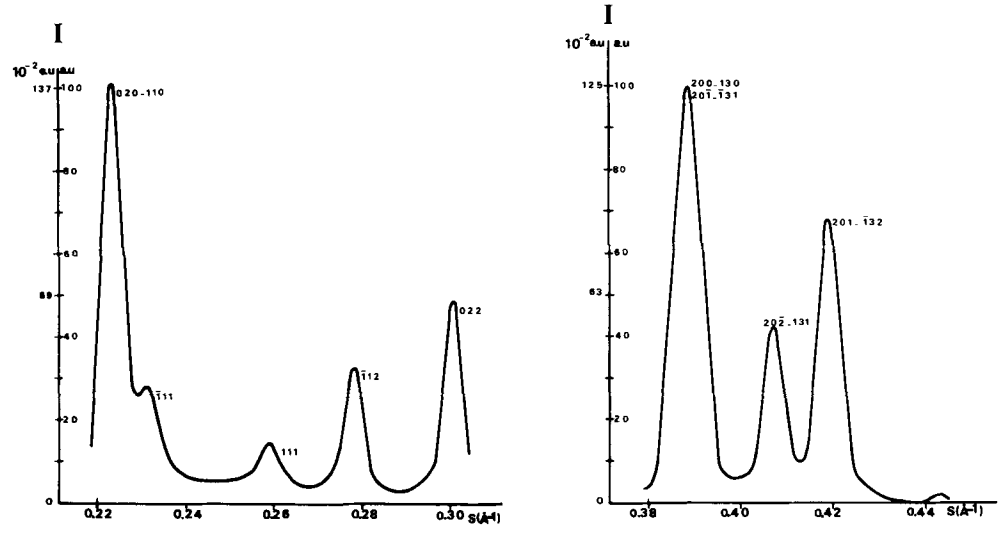

FIG. 5. Calculated profiles for an *I* stacking: (a) 02*l*, 11*l* reflections; (b) 20*l*, 13*l* reflections.

phenomenon is due to approximately the same values of $\vec{t_0}$ translations in *C*, *M* and *I* stacking and very different values in *T* stacking. The variation of atomic coordinates between *T*, *C* and *M* stacking does not influence greatly the structure factor for 20*l*, 13*l* reflections as can be seen in Table 2. It is interesting to note that in the cases of *M* and *I* stackings there are considerable variations in the distribution of intensities along each individual rod, but this difference partly disappears in powder profiles. This effect is achieved by the summation of the intensities of six *hk* rods in the powder diagram.

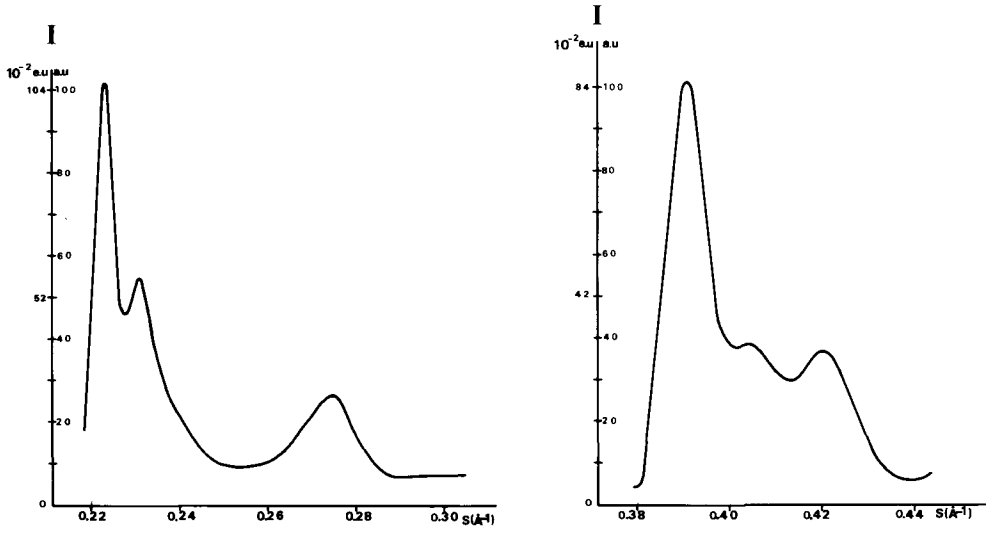

FIG. 6. Calculated profiles for a T stacking with 50% arbitrary faults: (a) (02, 11) band; (b) (20, 13) band.

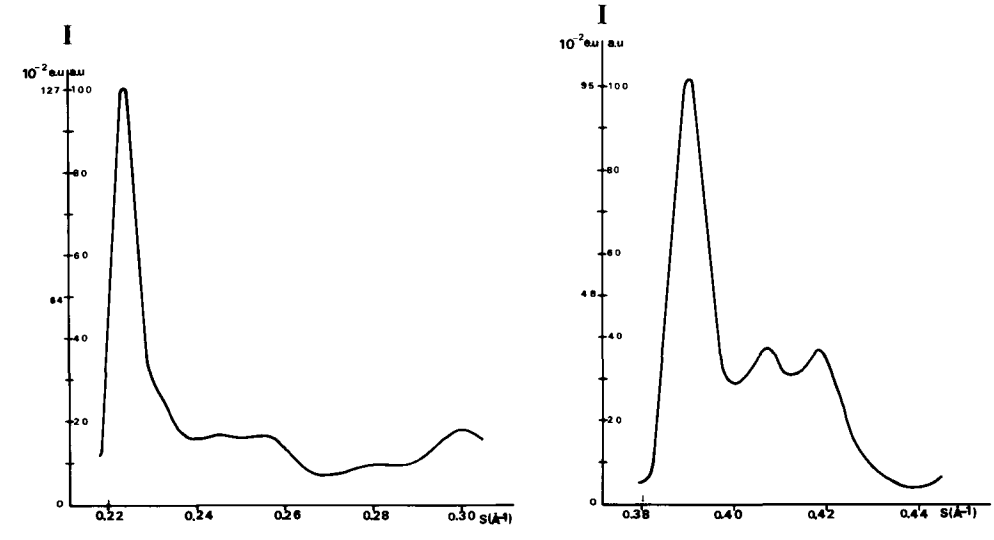

FIG. 7. Calculated profiles for a C stacking with 50% arbitrary faults: (a) (02, 11) band; (b) (20, 13) band.

Intensity distribution for T, C, M and I stacking with only arbitrary stacking faults

The introduction of arbitrary stacking faults in T, C, M and I stackings modifies hkl profiles, but the main diffraction features described in the previous section are preserved and still permit one to distinguish between all these models. More important differences are visible in the $02(l)$, $11(l)$ profiles. This can be seen qualitatively in Figs 6–9 where the value of 50% is taken for the abundance p of arbitrary faults for each type of stacking.

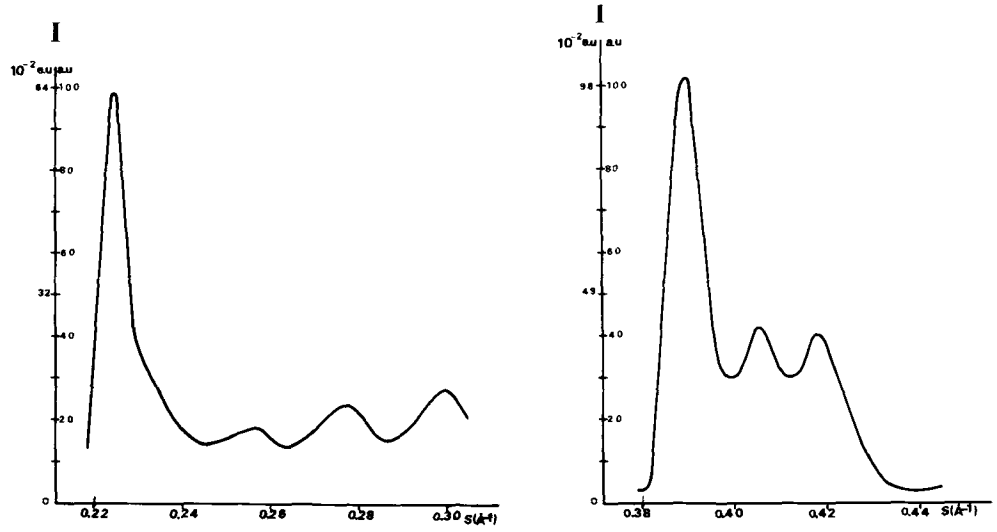

FIG. 8. Calculated profiles for an M stacking with 50% arbitrary faults: (a) (02, 11) band; (b) (20, 13) band.

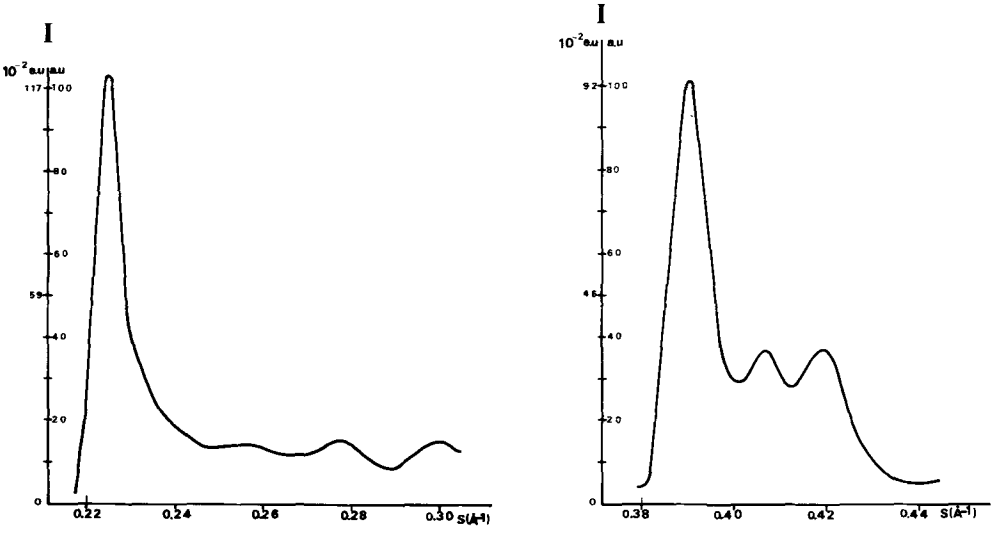

FIG. 9. Calculated profiles for an I stacking with 50% arbitrary faults: (a) (02, 11) band; (b) (20, 13) band.

When the p value increases the differences in the (02, 11) band profiles progressively disappear and T, C and I stackings with $p = 100\%$ produce an identical distribution of intensities for this diffraction domain. On the contrary, an M model can be easily distinguished from the other three as the intensity of the (02, 11) domain is reduced by half: Figs 10 and 11 compare the (02, 11) bands for M and I structures with $p = 100\%$. For T and C models two dimensional (02, 11) bands are identical but the profiles of (20, 13) bands are different.

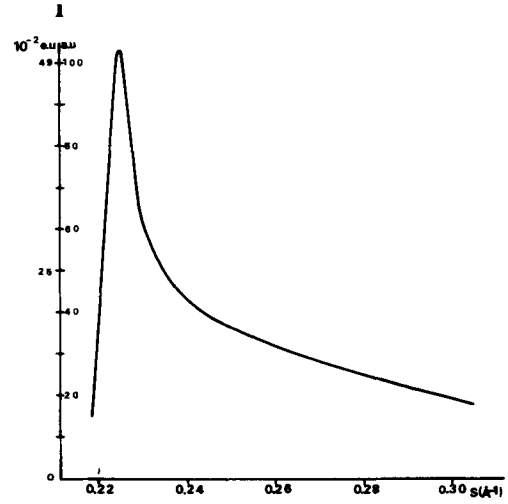

FIG. 10. Calculated (02, 11) band for an M stacking with 100% arbitrary faults.

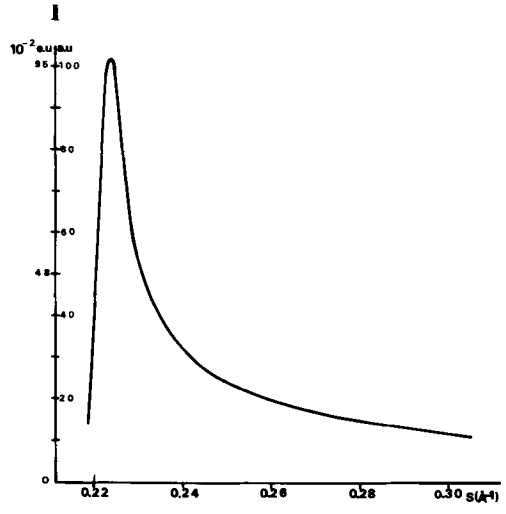

FIG. 11. Calculated (02, 11) band for an I stacking with 100% arbitrary faults.

The introduced arbitrary faults can be obtained by arbitrary rotations of adjacent layers or their translations in any direction with any value. However, we may obtain close results when we introduce a distribution of the interlayer displacements values around the initial $\vec{t}_0$. For example, Figs. 12 and 13 show the (20, 13) profile for a C stacking in the case of a Gaussian distribution of the $\vec{t}$ values with a half-width equal to 0·1 Å (Fig. 12) and with arbitary faults when $p = 25\%$ (Fig. 13). Interestingly, a distribution of the values of translations around $\vec{t}_0$ (in the $\vec{a}$ direction) modifies only the hk reflections with $h \neq 0$, while a distribution in the $\vec{b}$ direction will influence only the reflections with $k \neq 0$. Such an approach thus gives a possibility for selective change of the profiles in different domains of a calculated diagram.

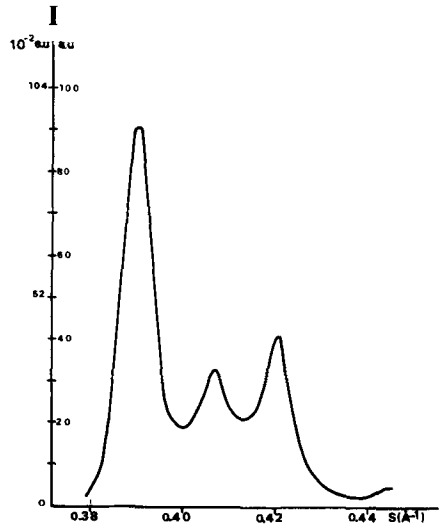

FIG. 12. Calculated (20, 13) band for a *C* stacking with a Gaussian distribution of the $\vec{t}$ values with a half-width equal to 0·1 Å.

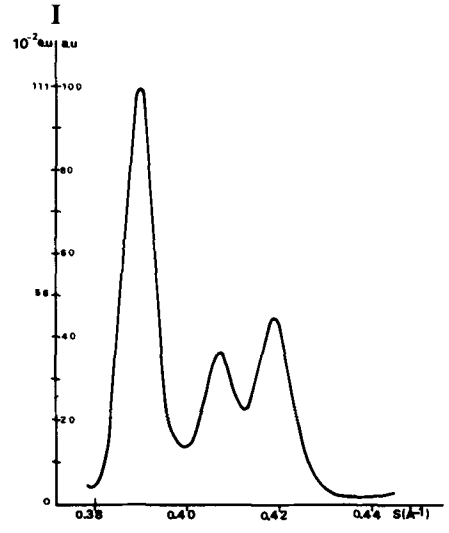

FIG. 13. Calculated (20, 13) band for a *C* stacking with 25% arbitrary faults.

Stackings with rotational ±120° and translational $\pm\vec{b}/3$ faults

We have previously shown that the existence of $\pm\vec{b}/3$ defects modifies the interlayer distances, whereas this phenomenon does not take place in the case of ±120° rotational faults. Our investigations have shown that the presence of different basal distances, varying between 10 and 10·8 Å in the case of K cations, changes slightly the positions of the *hkl* diffraction maxima, but preserves the main features of distribution of the intensities that corresponds to each model. Therefore in the next sections we will not emphasize the modifications caused by a variation of basal distances.

It is well known that the existence of $\pm 120°$ rotational or $\pm\vec{b}/3$ translational defects modifies (02, 11) profiles and has a little or no influence on the (20, 13) domain for C, M and I stackings. Our problem was only to establish whether it is possible to distinguish these two kinds of stacking faults when the models contain a high concentration of such defects. The calculations have shown that:

1. T stacking containing $\pm 120°$ rotational faults can be easily distinguished from the one with $\pm\vec{b}/3$ defects on the basis of the (20, 13) domain which is strongly modified in the case of rotational faults.

2. By examination of the (02, 11) domain we can distinguish between C, M and I models and determine the nature of stacking faults ($\pm 120°$ or $\pm\vec{b}/3$) in them even when their abundance is at a maximum ($\eta = 0{\cdot}67$). Figs 14a and b, show the difference in the

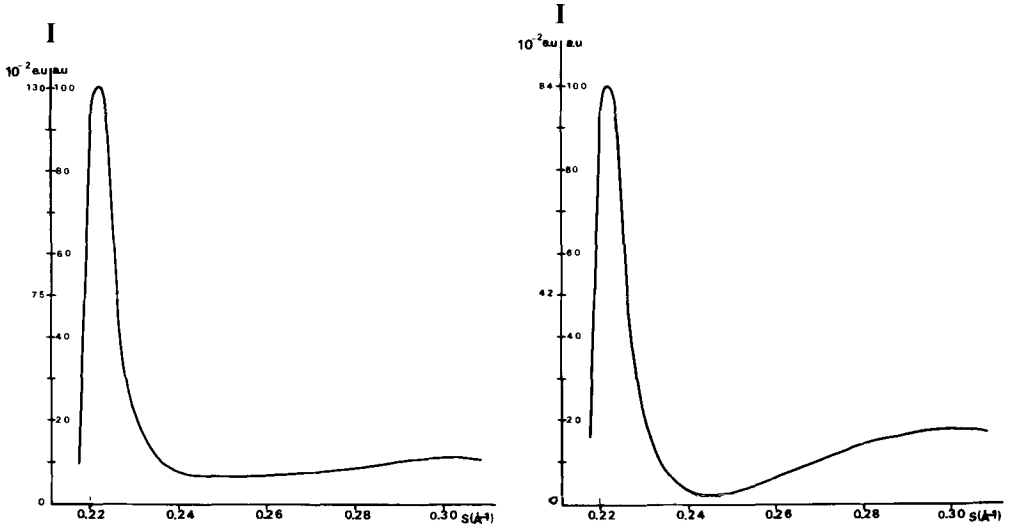

FIG. 14. Calculated (02, 11) band for stackings with $\pm 120°$ rotational faults ($\eta_R = 0{\cdot}67$): (a) C stacking; (b) M stacking.

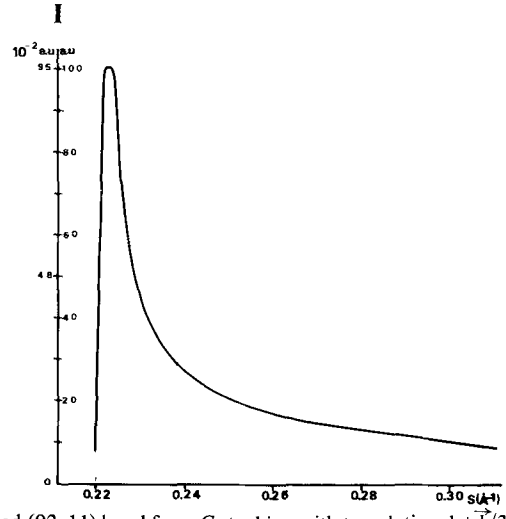

FIG. 15. Calculated (02, 11) band for a C stacking with translational $\pm\vec{b}/3$ faults ($\eta_T = 0{\cdot}67$).

(02, 11) band profiles which have been calculated for the same types of faults ($\pm 120°$) but different kind of layers (*C* stacking and *M* stacking), while comparison of Fig. 14a and Fig. 15 shows the profile modifications for a *C* stacking containing rotational and translational defects. We also observed differences in absolute values of the intensities. It is important to emphasize that the presence of rotations $\pm 120°$ can be distinguished from the $\pm\vec{b}/3$ translations by study of the (02, 11) band. The characteristic effect of the presence of translational $\pm\vec{b}/3$ faults appears in the regular decrease of the intensity after maximum value (as in the case of a 2*D* structure) while the rotational $\pm 120°$ leads to the presence of a more or less important minimum in the intensity near $s = 0{\cdot}24$ Å^{-1}.

3. The introduction of arbitrary displacements into a model with $\pm 120°$ defects can bring about a (02, 111) profile similar to those obtained with the model with only the $\pm\vec{b}/3$ faults; in these cases, however, the two (20, 13) domains are considerably different.

Stacking with rotational n60° and translational $-n\vec{a}/3 \pm m\vec{b}/3$ faults

Rotational n60° defects. Suppose that models with n60° faults are mica-like stackings (K cations are always between two adjacent 'hexagonal' cavities). Then the translations between adjacent layers are :

For layers with 0° and 180° rotations $\vec{t} = \mp\vec{a}/3$.
For layers with $\pm 60°$ rotations $\vec{t} = +\vec{a}/3 \pm \vec{b}/3$.
For layers with $\pm 120°$ rotations $\vec{t} = -\vec{a}/3 \pm \vec{b}/3$.

Figs 16 and 17 give the (02, 11) and (20, 13) band profiles in the case of *C* stacking with different concentrations of rotational faults. We observe, as the main effect, the overlapping of the two series of reflections $20\bar{2}$, 131 and 201, $\bar{1}32$ when the abundance of layer rotations increases. In the series of 02(l), 11(l) reflections, a small amount of defects ($\eta_R = 0{\cdot}33$) leads to a strong decrease of intensities for all reflections relative to the 020, 110 ones. When the concentration of defects increases ($\eta_R = 0{\cdot}67$), we observe a (02, 11) band profile with noticeable modulation near $s = 0{\cdot}30$ Å^{-1}.

The comparison between these profiles and those given by different models of *C* stacking previously discussed permits us to conclude that models with *n*60° rotational faults can be distinguished from the others without ambiguity. For example, comparison of Figs 16b and 7b (*C*-stacking + arbitrary faults) shows, in both cases, three modulations, but absolute intensities and the value of the minimum near $s = 0{\cdot}40$ Å^{-1} are very different.

The introduction of arbitrary stacking faults into the model with *n*60° rotational defects gives a development of 02(l), 11(l) reflections (Fig. 18a) similar to the increase of η_R (Fig. 17a). But as the (20, 13) band (Fig. 18b) has another profile (compared with Fig. 17b), a quantitative comparison between experimental data and calculated curves will permit determination of the value of η_R even in the presence of arbitrary stacking faults.

C models containing translational defects with $-n\vec{a}/3 \pm m\vec{b}/3$ stacking faults. First we will examine models where there exist (simultaneously and with the same probability $\eta_T/2$) stacking faults corresponding to additional translations equal to $-\vec{a}/3 + \vec{b}/3$ and $-\vec{a}/3 - b/3$. Such faults lead to a stacking where adjacent faulted layers have a pyrophyllite-like interlayer configuration (K cations are in the 'hexagonal' cavities of one layer and are coordinated with only one oxygen atom of the neighbouring layer). Calculated band profiles from models of this type show that even for a small number of translational faults the $20\bar{2}$, 131 and 201, $\bar{1}32$ reflections overlap. In the series of 02(l), 11(l) reflections, we observe a

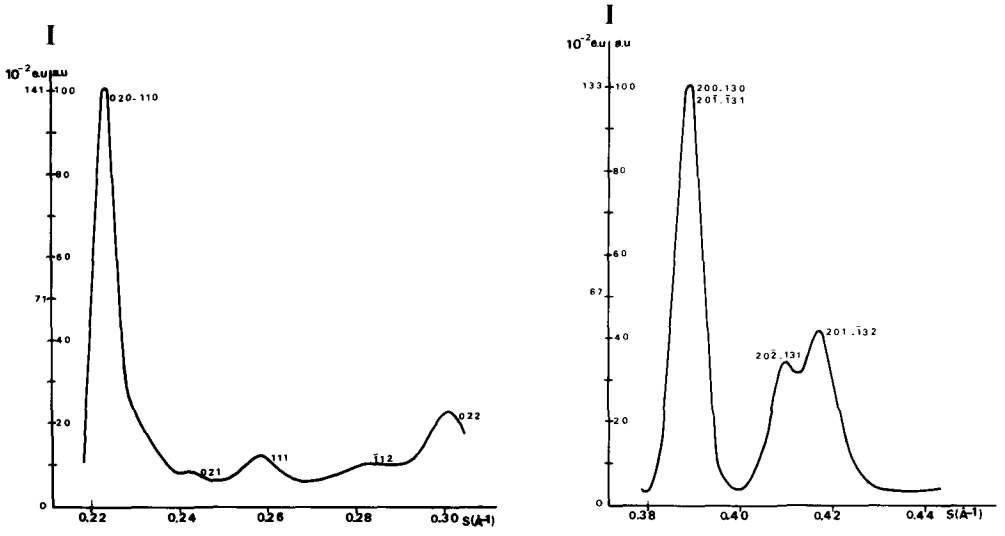

FIG. 16. Calculated profiles for a C stacking with $\pm n60°$ rotational faults ($\eta_R = 0{\cdot}33$): (a) (02, 11) band; (b) (20, 13) band.

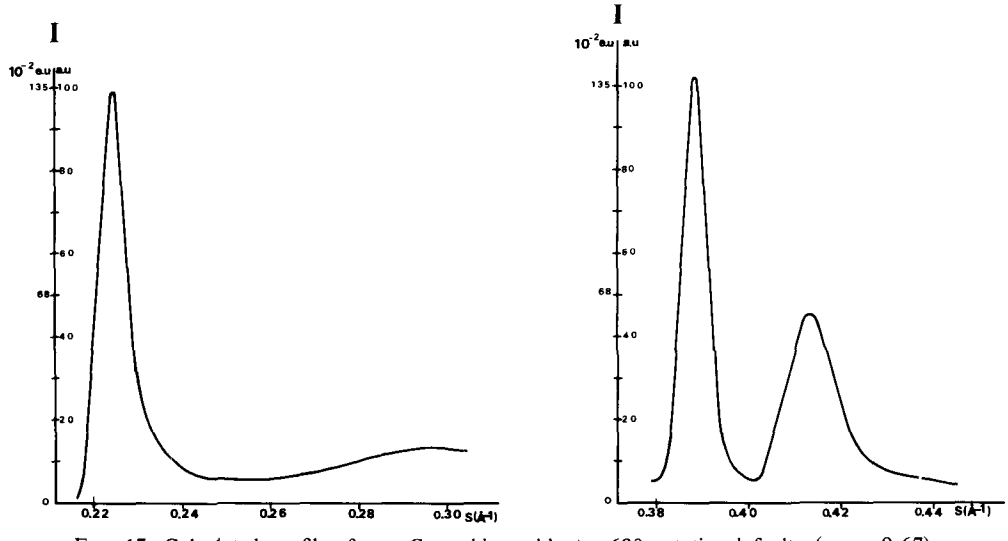

FIG. 17. Calculated profiles for a C stacking with $\pm n60°$ rotational faults ($\eta_R = 0{\cdot}67$): (a) (02, 11) band; (b) (20, 13) band.

relative increase of the reflections at $s \# 0{\cdot}26$ Å^{-1} and $s \# 0{\cdot}28$ Å^{-1}, and a sharp decrease of the reflection at $s \# 0{\cdot}30$ Å^{-1}. Figs 19 and 20 illustrate these peculiarities for $\eta_T = 0{\cdot}33$ and $\eta_T = 0{\cdot}67$. These diffraction features permit the distinction of this kind of fault from $\pm 120°$ and $n60°$ rotational defects and from C stacking with only arbitrary faults.

The more general probability of $(-\vec{na}/3 \pm \vec{mb}/3)$ stacking faults corresponds to the case when $n = 0$ or 1 and $m = 0$ or 1, which results in stackings with five additional

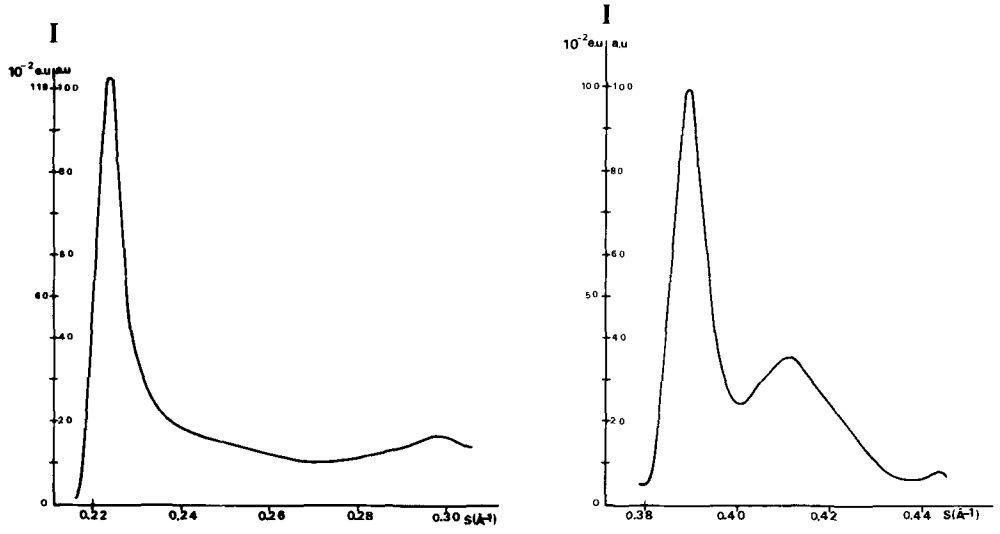

FIG. 18. Calculated profiles for a *C* stacking with $\pm n60°$ rotational faults ($\eta = 0{\cdot}33$) and with 50% of arbitrary faults: (a) (02, 11) band; (b) (20, 13) band.

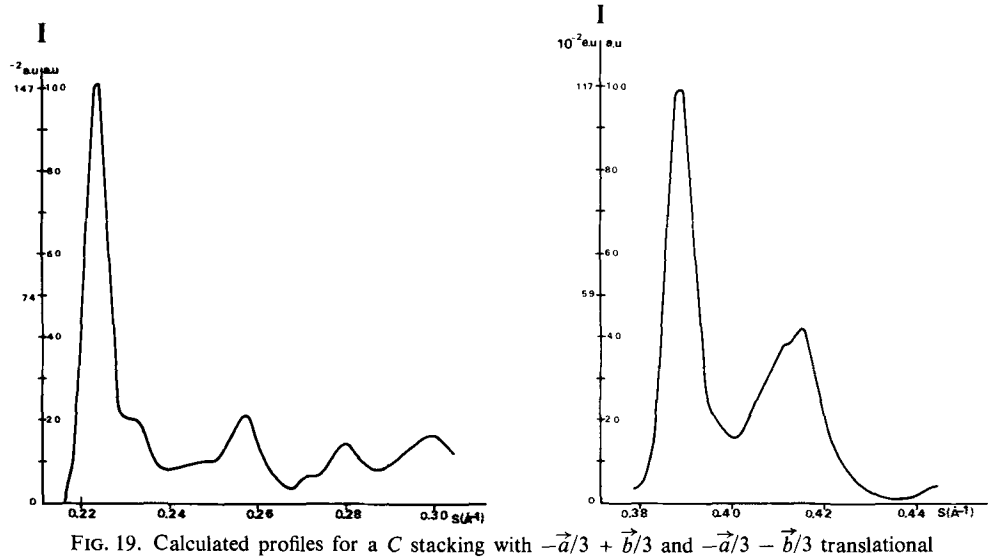

FIG. 19. Calculated profiles for a *C* stacking with $-\vec{a}/3 + \vec{b}/3$ and $-\vec{a}/3 - \vec{b}/3$ translational faults ($\eta_T = 0{\cdot}33$); (a) (02, 11) band; (b) (20, 13) band.

translational displacements having the same probability $\eta_T/5$ and equal to: $0 \pm \vec{b}/3$; $-\vec{a}/3 \pm \vec{b}/3$ and $-\vec{a}/3 + 0$. We observe that these additional displacements between adjacent layers lead to the same set of translations as in *C* stacking with $n60°$ rotational faults. The existence of the $(-n\vec{a}/3 \pm m\vec{b}/3)$ translational defects leads to two different coordinations for K cations:

The first one as in the model described above, with only two kinds of translational faults. It corresponds to the $(-\vec{a}/3 \pm \vec{b}/3)$ and $-\vec{a}/3$ additional translations.

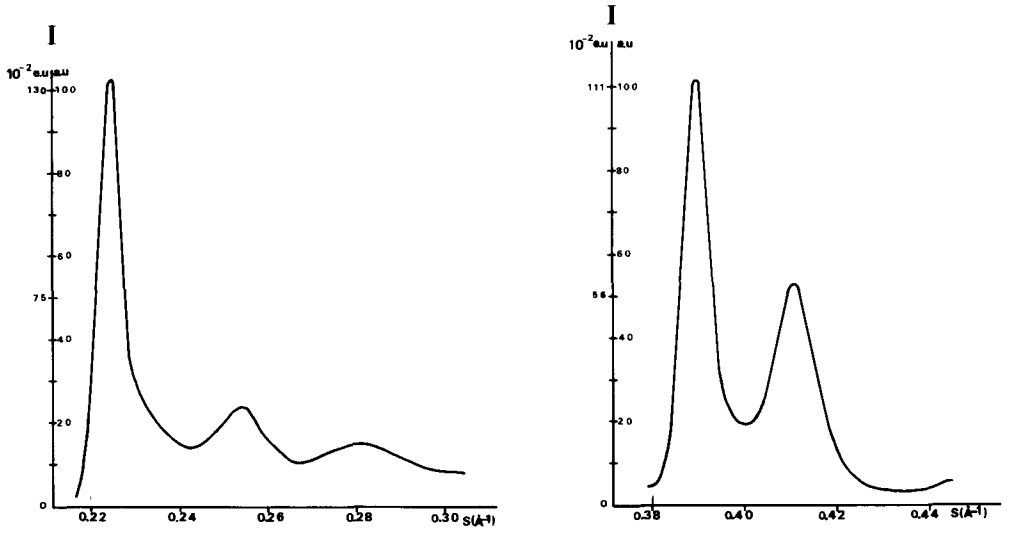

FIG. 20. Calculated profiles for a C stacking with $-\vec{a}/3 + \vec{b}/3$ and $-\vec{a}/3 - \vec{b}/3$ translational faults ($\eta_T = 0{\cdot}67$): (a) (02, 11) band; (b) (20, 13) band.

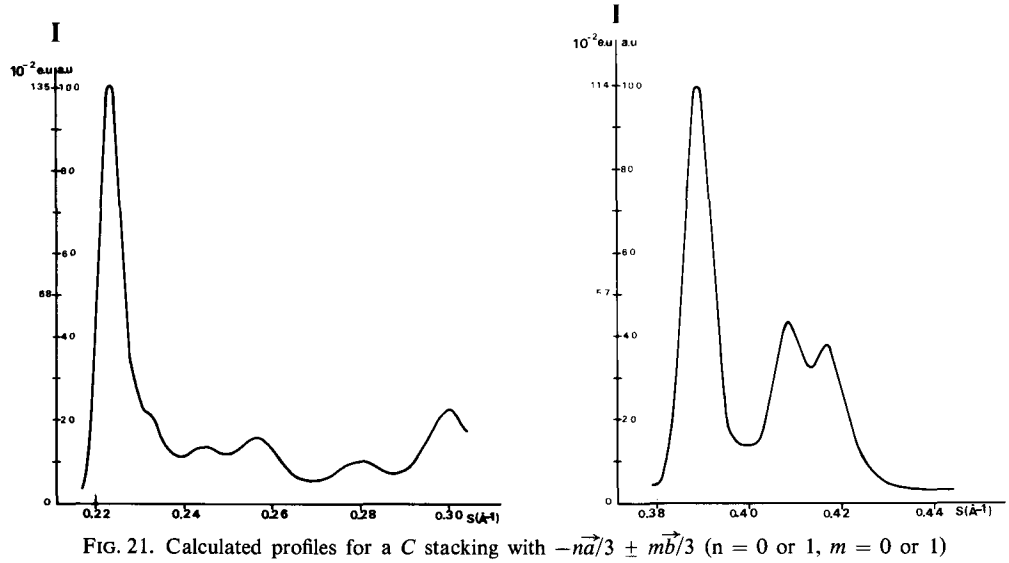

FIG. 21. Calculated profiles for a C stacking with $-n\vec{a}/3 \pm m\vec{b}/3$ (n = 0 or 1, m = 0 or 1) translational faults ($\eta_T = 0{\cdot}33$): (a) (02, 11) band; (b) (20, 13) band.

The second coordination, caused by $\pm\vec{b}/3$ additional translations, in which K cations are in 'hexagonal' cavities of one layer and are coordinated with three oxygen atoms forming the base of a tetrahedron of the neighbouring layer.

Figs 21 and 22 show that the increase in the abundance of η_T leads to the overlapping of the $20\bar{2}$, 131 and 202, $\bar{1}32$ reflections and a decrease in the 02(l), 11(l) ones ($l \neq 0$), with their relative intensities preserved.

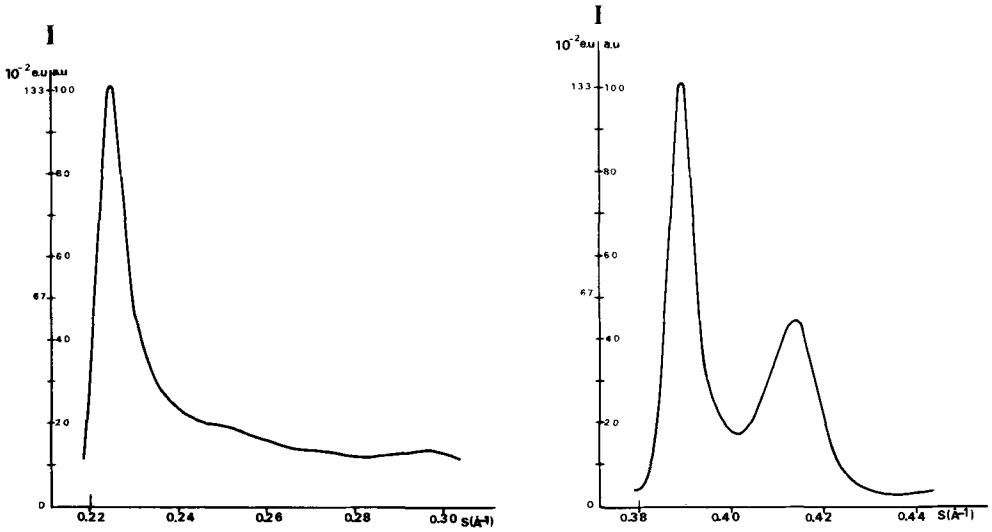

FIG. 22. Calculated profiles for a *C* stacking with $-n\vec{a}/3 \pm m\vec{b}/3$ ($n = 0$ or 1, $m = 0$ or 1) translational faults ($\eta_T = 0{\cdot}67$): (a) (02, 11) band; (b) (20, 13) band.

Comparison between these profiles and those obtained from *C* stacking with arbitrary faults, on the one hand, and with $n60°$ rotations, on the other, leads to the following conclusions:

(a) *C* stacking with arbitrary faults is easily distinguishable from a stacking with $(-n\vec{a}/3 \pm m\vec{b}/3)$ faults on the basis of $20(l)$, $13(l)$ band profiles, whereas $02(l)$, $11(l)$ band profiles may be similar in the two models for particular values of fault abundances.

(b) The differences between the calculated profiles are not so evidence in the case of models containing either $n60°$ rotations or the $(-n\vec{a}/3 \pm m\vec{b}/3)$ faults. This difficulty grows with increase in defect abundance.

CONCLUSIONS

The principal parameters of the modification of the intensity distribution studied in this investigation were: the nature of the layer (*T*, *C*, *M* layers), their stacking (*T*, *C*, *M*, or *I* stackings), types of stacking faults which appear as the most frequently described and the most probable from a crystallochemical point of view.

1. The distribution of intensities for the $02(l)$, $11(l)$ bands permits differentiation, without ambiguity, between *T*, *C*, *M* or *I* stackings even in the presence of stacking faults. Particularly in the case of *M* and *I* stackings, relative intensities are similar but the absolute values of intensities of $02l$, $11l$ reflections are always different by a factor of two as well as when the abundance of arbitrary faults is $p = 0$ or $p = 1$.

2. The stacking faults have been classified into three categories: (i) arbitrary translations and/or rotations; (ii) $\pm 120°$ or $\pm\vec{b}/3$ defects; (iii) $n60°$ or $-n\vec{a}/3 \pm m\vec{b}/3$ faults. This study has shown that each category can be distinguished if we analyse simultaneously the (02, 11) and (20, 13) diffraction domains. The existence of arbitrary defects modifies specifically all the diagrams except $00l$ reflections. The presence of $\pm 120°$

or $\pm\vec{b}/3$ faults preserves the distribution of intensities of the (20, 13) bands in the case of C, M and I stackings (stackings where $t_0 \neq -\vec{a}/3$). For T stackings, $\pm 120°$ faults modify this diffraction domain but lead to (20, 13) profiles which differ from those obtained with arbitrary defects. The third category of stacking faults can easily be distinguished from the second one which gives few (or no) modifications of the (20, 13) domain. On the contrary, the presence of $n60°$ or $-n\vec{a}/3 \pm m\vec{b}/3$ defects leads to specific variations of this domain with the overlapping of reflections $20\bar{2}$, 131 and 201, $\bar{1}32$ caused by their shift to a mean position: this effect is absent in the case of arbitrary faults.

3. It has proved easy to distinguish the $\pm 120°$ stacking faults from the $\pm\vec{b}/3$ ones in the case of the T model. The presence of $\pm\vec{b}/3$ defects does not modify the distribution of intensities for $20l$, $13l$ reflections, whereas the existence of $\pm 120°$ rotations changes considerably the profile of bands of this diffraction domain (this effect is related to the value of the $\vec{t}_0$ translation which is noticeably different from $-\vec{a}/3$ in a T stacking). The differences in (20, 13) profiles will not be so evident if the stackings are of C, M or I type because in these cases the values of $\vec{t}_0$ translations are rather close to $-\vec{a}/3$. However the $\pm 120°$ and $\pm\vec{b}/3$ faults can be distinguished by a quantitative study of the (02, 11) diffraction domain whatever the proportion of such faults.

4. The comparison between models containing $n60°$ and $-n\vec{a}/3 \pm m\vec{b}/3$ has shown that the differences in the profiles, for the (02, 11) domain as well as for the (20, 13) domain, are not very sensitive. The detection of stackings with a large proportion of such defects, or when arbitrary faults are added, proves especially difficult.

5. When the studied smectites are saturated by cations with large ionic radii it is possible to distinguish between models with rotational and translational faults by a fine analysis of the distribution of intensities along the 00 rod. The presence of tranlational defects in such smectites is accompanied by the appearance of several interlayer distances leading to a distribution of intensity as in mixed-layer structures.

6. It is important to note that the distribution of intensities in the (20, 13) diffraction domain depends very strongly on the value of the $\vec{t}_0$ translation. For example, different $20l$, $13l$ reflections have comparable intensities for C, M and T models (as can be seen in Table 2); however the powder (20, 13) profiles are not the same, in the presence of a large amount of stacking faults, because of the differences of the $\vec{t}_0$ values in T and C or M models. Such features allow us to predict the type of stacked layers.

Finally, if we compare good experimental diffraction patterns with the theoretical ones given in this paper it is possible to recognize the nature of the layers and of the stacking faults. However, to obtain the concentration of principal parameters characterizing each model it is necessary in all cases (i) to measure very accurately the distribution of intensities and their positions in all accessible parts of the reciprocal space and (ii) to fit quantitatively the calculated pattern with the experimental one, not only on the basis of profile accordance but also by comparing the intensity values. Obviously, the better the ordering of the stacking, the better the solution will be.

REFERENCES

BAILEY S.W. (1966) Status of clay mineral structures. *Clays Clay Miner.* **26,** 3–21.

BESSON G. (1980) *Structures des smectites dioctaédriques. Paramètres conditionnant les fautes d'empilement des feuillets.* Thesis, Univ. Orléans, France.

BESSON G., GLAESER R. & TCHOUBAR C. (1983) Le césium, révélateur de structure des smectites. *Clay Miner.* **18,** 11–19.

BRINDLEY G.W. & BROWN G. (1980) *Crystal Structures of Clay Minerals and their X-ray Identification.* Mineralogical Society, London.

DRITS V.A. & SAKHAROV B.A. (1976) *X-ray Analysis of Mixed-Layer Minerals* (in Russian). Ed. Nauka, Moscow.

GÜVEN N. & PEASE R.W. (1975) Selected area electron diffraction studies on beidellite. *Clay Miner.* **10,** 427–436.

MAMY J. & GAULTIER J.P. (1976). Les phénomènes de diffraction des rayonnements X et electroniques par les réseaux atomiques. Application à l'étude de l'ordre cristallin dans les minéraux argileux. II: Evolution structurale de la montmorillonite associée au phénomène de fixation irréversible du potassium. *Ann. Agron.* **27 (I),** 1–16.

MERING J. & OBERLIN A. (1967) Electron-optical study of smectites. *Clays Clay Miner.* **15,** 3–25.

PLANÇON A. (1976) *Phénomène de diffraction produit par les systèmes stratifiés comportant simultanément des feuillets de natures différentes et des fautes d'empilement. Application à l'étude qualitative et quantitative des défauts dans les kaolinites partiellement désordonnées.* Thesis, Univ. Orléans, France.

PLANÇON A. (1981) Diffraction by layer structures containing different kinds of layers and stacking faults. *J. Appl. Cryst.* **14,** 300–304.

PLANÇON A. & TCHOUBAR C. (1976) Etude des fautes d'empilement dans les kaolinites partiellement désordonnées. II: Modèles d'empilement comportant des fautes par rotation. *J. App. Cryst.*, **9,** 279–285.

PLANÇON A. & TCHOUBAR C. (1977a) Determination of structural defects in phyllosilicates by X-ray powder diffraction. I: Principle of calculation of the diffraction phenomenon. *Clays Clay Miner.* **25,** 430–435.

PLANÇON A. & TCHOUBAR C. (1977b) Determination of structural defects in phyllosilicates by X-ray powder diffraction. II: Nature and proportion of defects in natural kaolinite. *Clays Clay Miner.* **25,** 436–450.

PLANÇON A., BESSON G., GAULTIER J.P., MAMY J. & TCHOUBAR C. (1979) Qualitative and quantitative study of structural reorganization in montmorillonite after potassium fixation. *Proc. VIth Int. Clay Conf. Oxford 1978*, 45–54.

SAKHAROV B.A., NAUMOV A.S. & DRITS V.A. (1982a) X-ray diffraction by mixed-layer structures with random distribution of stacking faults (in Russian). *Dok. Akad. Nauk.* **265,** 339–343.

SAKHAROV B.A., NAUMOV A.S. & DRITS V.A. (1982b) X-ray intensities scattered by layer structure with short range ordering parameters $S \geqslant 1$ and $G \geqslant 1$ (in Russian). *Dok. Akad. Nauk.* **265,** 871–874.

TSIPURSKY S.I. (1982) *Determination of structural and crystallochemical features of dioctahedral micas and smectites by means of oblique texture electron diffraction* Thesis n° 040020, Moscow, USSR (in Russian.)

TSIPURSKY S.I. & DRITS V.A. (1977) Efficiency of method of the direct measurement of intensity in structural determination by means of oblique texture electron diffraction (in Rusian). *Isvestia Acad. Nauk. Physical Series* **11,** 2263–2271.

TSIPURSKY S.I., DRITS V.A. & TCHECKIN S.S. (1978) Determination of structure ordering in nontronites by means of oblique texture electron diffraction, (in Russian). *Isvestia Acad. Nauk. Geol. Series* **10,** 105–113.